Correlation between non-spectral and cumulative-based ground motion intensity measures and demands on structures under mainshock-aftershock seismic sequences considering the effects of incident angles

Saeed Amiri[1], Luigi Di Sarno[2, 3],Alireza Garakaninezhad[4]

[1] Department of Civil, Geological and Mining Engineering, Polytechnique Montreal, Montreal, QC, Canada
E-mail address: saeed.amiri@polymtl.ca
[2] University of Liverpool, School of Engineering, Department of Civil Engineering and Industrial Design, Liverpool, UK
E-mail address: luigi.di-sarno@liverpool.ac.uk
[3] Department of Engineering, University of Sannio, Benevento, Italy
E-mail address: ldisano@unisannio.it
[4]Department of Civil Engineering, Faculty of Engineering, University of Jiroft, Jiroft, Kerman, Iran
E-mail address: a.garakani@ujiroft.ac.ir

Abstract

One of the pivotal steps in seismic assessment of structures is the definition of functional relationships between Engineering Demand Parameter (EDP) and an ground motion Intensity Measure (IM). This paper investigates the correlation between widely used non-spectral and cumulative-based ground motion intensity measures and corresponding engineering demand parameters for regular and irregular structures as bidirectional single-degree-of-freedom (2D-SDOF) systems. Such correlation is investigated under sequential earthquakes in terms of efficiency and sufficiency, considering various seismic incident angles. Structural performance is expressed as maximum inelastic displacement, *MD*, maximum inelastic absolute acceleration, *MA*, residual displacement, *RD*, and hysteretic energy, *EH*. The results of the extensixe parametric analysis show that if the *MD*, *MA*, *EH* and *RD* of regular systems are considered as demand parameters, the optimal IMs in terms of efficiency and sufficiency are v_{sq}, a_{rms}, v_{rs} and v_{sq}, respectively.

Keywords: Seismic incident angle, Mainshock-aftershock sequences, Efficiency and sufficiency of Intensity Measures, Engineering demand parameters.

1. Introduction

Numerous aftershocks can be triggered by a strong mainshock due to both static stress and dynamic stress changes occurring during fault mechanism generating ground motions. Mainshock-damaged structures are more vulnerable to severe damage or even collapse during aftershocks. The past earthquakes showed that mainshock-aftershock sequences can cause major disasters and, in turn, lead to significant economic losses. For instance, about 42,719 aftershocks occurred after the 2008 Wenchuan, China mainshock earthquake (M_w=7.9). More than 70,000 victims were reported in the Wenchuan earthquake and its aftershocks. In addition, the economic loss induced by this earthquake was estimated to be around $150 billion. 24 hours after the earthquake in Chile (M_w=8.8) on February 27, 2010, approximately 90 aftershocks with magnitudes equal to or larger than 5.0 were recorded, and the total economic loss was estimated at $30 billion [1].

After the 2011 great Tohoku earthquake in Japan with M_w=9.0, around 588 aftershocks with magnitudes equal to or larger than 5.0, 60 aftershocks with magnitudes larger than 6.0 and three over 7.0 were recorded. As a result, 15,782 deaths, 240,332 half destroyed and 128,530 totally destroyed houses were documented due to these seismic sequences and resulting tsunami [2]. The destructive east Indian Ocean earthquake struck Indonesia on April 11, 2012, with moment magnitude 8.6 (M_w=8.6), followed by several strong aftershocks with the largest measured at M_w=8.2 just over two hours later [3]. In recent years, several sequential earthquakes took place, such as the 2016 Central Italy earthquake [4], the 2017 Ezgeleh-Sarpole-Zahab earthquake in Iran [5], and the Haiti Earthquake in 2021 [6], which imposed major structural damage. It is therefore of paramount importance to investigate the effects of multiple earthquakes on seismic

performance of structures and infrastructure. Note that frequency content characteristics and duration of the mainshock and the corresponding aftershock can differ significantly. Meanwhile, a strong correlation is observed between the mean occurrence rate and the distribution of aftershocks with the mainshock magnitude.

Several studies have addressed the seismic assessment of structures under seismic sequences by focusing on single-degree-of-freedom (SDOF) [7-11], and multiple-degree-of-freedom (MDOF) [12-18] systems. It should be pointed out that current seismic codes don't consider sequential ground motions to design of structures.

The earthquake incident angle plays a significant role on seismic performance of structures. The majority of preiovus works have focused on the effects of seismic incident angle on the seismic response of structures (e.g. [19-28]). A limited number of researchers examined the seismic behavior of structures against multiple earthquakes considering the effect of seismic incident angle [29-35].

Hatzivassiliou and Hatzigeorgiou [29] evaluated the seismic performance of four three-dimensional reinforced concrete (RC) structures (two regular and two irregular buildings) under five real seismic sequences using nonlinear dynamic analyses. Irregular buildings were analyzed for different sitting configurations to investigate the effect of earthquake incident angle were considered. It was found that ductility demands strongly depend on the direction of earthquakes applied to the buildings.

Recently, Kostinakis and Morfidis [31] addressed the impact of seismic sequences on the damage level of 3D multi-story RC buildings with various structural systems taking into account the influence of incident angles on the structural response. To this aim, six medium-rise RC buildings were studied under 40 single ground motions as well as for 80 bidirectional seismic sequences. The results revealed that the incident angle can drastically affect the

successive earthquake, depending on characteristics of the structure, number of the repeated strong motions, and distance of the record from the fault.

Hosseinpour and Abdelnaby [36] assessed the seismic performance of two eight-story RC buildings (regular and irregular) subjected to 2010–2011 Christchurch multiple earthquakes taking into account the ground motion directionality influence. For this purpose, the sequences were applied in only two different directions and concluded that earthquake direction can affect the number of plastic hinges, drift and residual drift demands.

Omranian et al. [32] examined the fragility curves of a typical skew RC bridge located in California by considering the variety of different parameters such as incident angle and skew angle of deck under seismic sequences. Seven incident angles were taken in this regard. They demonstrated the direction of excitation plays a pivotal role in the seismic vulnerability of the skew bridge.

In another study, García et al. [33] investigated the seismic performance of 3D multi-story steel moment-resisting buildings (including or not including interior gravity frames) subjected to real mainshock-aftershock sequences with five different angles of incidence. This research showed that inter-story drift demand is dependent on earthquake direction and modeling approach of the 3D analytical models.

Wang et al. [34] evaluated the effect of ground motion directionality on seismic behavior of a typical concrete gravity dam-reservoir-foundation system under as-recorded multiple earthquakes. The sensitivity of the maximum structural demands was conducted for two different seismic incident directions. The results indicated that seismic damage propagation processes can be changed by considering the earthquake direction.

Moreover, Weiping Wen et al. [35] examined the necessity of rotating mainshock-aftershock sequences considering the change in the critical orientation. They assessed different seismic demands of nonlinear SDOF systems under an ensemble of rotated seismic sequences

as well as the variation of strength reduction factor, hysteretic models and relative aftershock intensity levels. This study revealed that aftershocks may change the seismic critical angle with respect to mainshocks, such that its value can increase by 30°. Additionally, rotating sequences is of paramount significance, increasing the responses to 25%.

More recently, Di Sarno et al. [37] investigated the effects of both directions of mainshock and subsequent aftershock on nonlinear demands of structures, as SDOF systems. They revealed that when incident angles of mainshock and aftershock would not be the same, more critical responses can be obtained. Additionally, Amiri et al. [38] examined the sufficiency of the aftershock polarity (positive and negative) in multiple earthquakes to determine maximum residual displacements of structures by considering relative differences between the incident angles of sequential ground motions.

Performance-Based Earthquake Engineering (PBEE) is an approach which aims to quantify the seismic performance of a structure using intensive but comprehensive nonlinear analyses. In this procedure, it is necessary to define a suitable Intensity Measure (*IM*) of ground motion which correlates reliably with an Engineering Demand Parameter (*EDP*) of a case study or portfolio of structure. Moreover, a successful correlation between the *IM* and *EDP* depends on the selection of an appropriate *EDP*, which should be a reliable indicator of the structural seismic response.

Numerous researchers have investigated the correlation between IMs and EDPs for buildings [39, 40], bridges [41-44] and pipelines [45-47] under single earthquakes. Limited studies have been performed to assess this correlation against multiple earthquakes [48, 49], in which only few numbers of IMs and EDPs have been taken into account. Moreover, in these studies, the effect of earthquake direction was ignored.

As mentioned above, there are a limited number of studies that have evaluated the effect of mainshock-aftershock sequences on inelastic responses of structures considering the seismic

incident angle. Also, only one research work has been conducted so far by the Authors [37] in this regard, in which the impacts of incident angles of both mainshock and subsequent aftershock are taken into account. In multiple earthquakes, the peak-based IMs, such as the Peak Ground acceleration (*PGA*), are not efficient ground motion indicators [48, 49], thus, considering the cumulative-based *IMs* can be effective in the correlation process. In addition, the appropriate selection of peak-based IM between mainshock, aftershock, and sequence, or their combination as a single IM can be a challenging task.

The objective of the present paper is to examine the correlation between a large number of non-spectral and cumulative-based ground motion IMs and different *EDPs* of the structures as 2D-SDOF systems under seismic sequences in terms of efficiency and sufficiency [50, 51], considering a wide variety of incident angle. In this study, the relative difference between directions of consecutive ground motions is considered as well.

2. Methodology

This paper investigates the correlation between different ground motion IM*s*, including non-spectral and cumulative-based ones, and a number of *EDPs* of 2D-SDOF systems with the elastic-perfectly plastic behavior model, when the angles of mainshock and subsequent aftershock can be different. As demonstrated in [37], if the directions of sequential ground motions would not be identical, the resulting structural nonlinear responses may be higher, compared to the situation where they are equal. Hence, this circumstance can lead to reliable seismic assessment of structures under multiple earthquake. The correlation in terms of efficiency and sufficiency is carried out herein in the case of 2D-SDOF systems having two principal structural axes, namely the X and Y direction. In this study, sequences with one mainshock and one aftershock are considered and then both mainshock and subsequent aftershock are rotated to different angles, which are not necessarily identical. Thus, the first step for the investigation, is generating rotated multiple earthquakes, such that there is a relative

difference between two consecutive incident angles. Afterwards, for rotated sequences related to each original multiple earthquake, *EDPs* are extracted from nonlinear time history analyses in various angles. Then, the maximum *EDP* obtained from all directions is accounted for as a representative response for that sequence. Obviously, the critical demand occurs at a specific combination of angles of mainshock and aftershock. This combination is considered as the directions corresponding to maximum *EDP*. Finally, efficiency and sufficiency analyses are carried out between the *IMs* values related to these directions, and the corresponding *EDPs* values for all earthquakes and structures considered in the paper. It is noted that that square-root-of-sum-of-squares (SRSS) method is used to obtain one unique value of *IM* and *EDP* from two perpendicular axes. The results are reported as the most efficient and sufficient *IM* for each *EDP* type in terms of response spectra and polar figures. Figure 1 shows the flowchart for the generation of rotated multiple earthquakes, so that each seismic shock is applied to structures with a specific angle. A procedure is then utilized to quantify maximum *EDPs* and then finding the most efficient and sufficient IM, which its flowchart is indicated in Figure 2.

It is worth noting that in this paper, *n*, the number of successive shocks in a seismic sequence is two, namely one mainshock and one aftershock. This is due, herein, for sake of brevity of results. The assessment will be more complicated if *n* is selected more than two, as discussed in [37]. Hence, each mainshock and subsequent aftershock are rotated from their initial orientation by angles θ_m , θ_a respectively. These angels can come from the same seismic source and hence may be dependent on each other, however, they are not necessarily identical with respect to each other. Thus, each earthquake excitation required for carrying out dynamic analysis is a seismic sequence with one mainshock rotated by the angle of θ_m , a time-interval of 50 sec possessing zero acceleration ordinates to stop the structure after the first event, and one succeeding aftershock rotated by the angle of θ_a. A wide range of incident angles is taken into account for both mainshock and aftershock, $\theta_m, \theta_a = 0^\circ, 10^\circ, 20^\circ, \ldots, 170^\circ, 180^\circ$. It is

apparent that the increment of both incident angles is 10° and as a result, $11 \times 11 = 121$ rotated seismic sequences are generated as input ground motions for dynamic analyses.

After performing analyses, the maximum value of *EDP* from 121 existing combinations is determined for two perpendicular horizontal components of earthquake. Then the SRSS method is employed to obtain one unique value as a representative damage measure of these cases. Moreover, the ground motion IM corresponding to the maximum *EDP* is specified. After that, the efficiency investigation using the Pearson correlation coefficient and also the sufficiency evaluation in terms of earthquake magnitude, $\boldsymbol{M_w}$ and epicentral distance, R, are conducted.

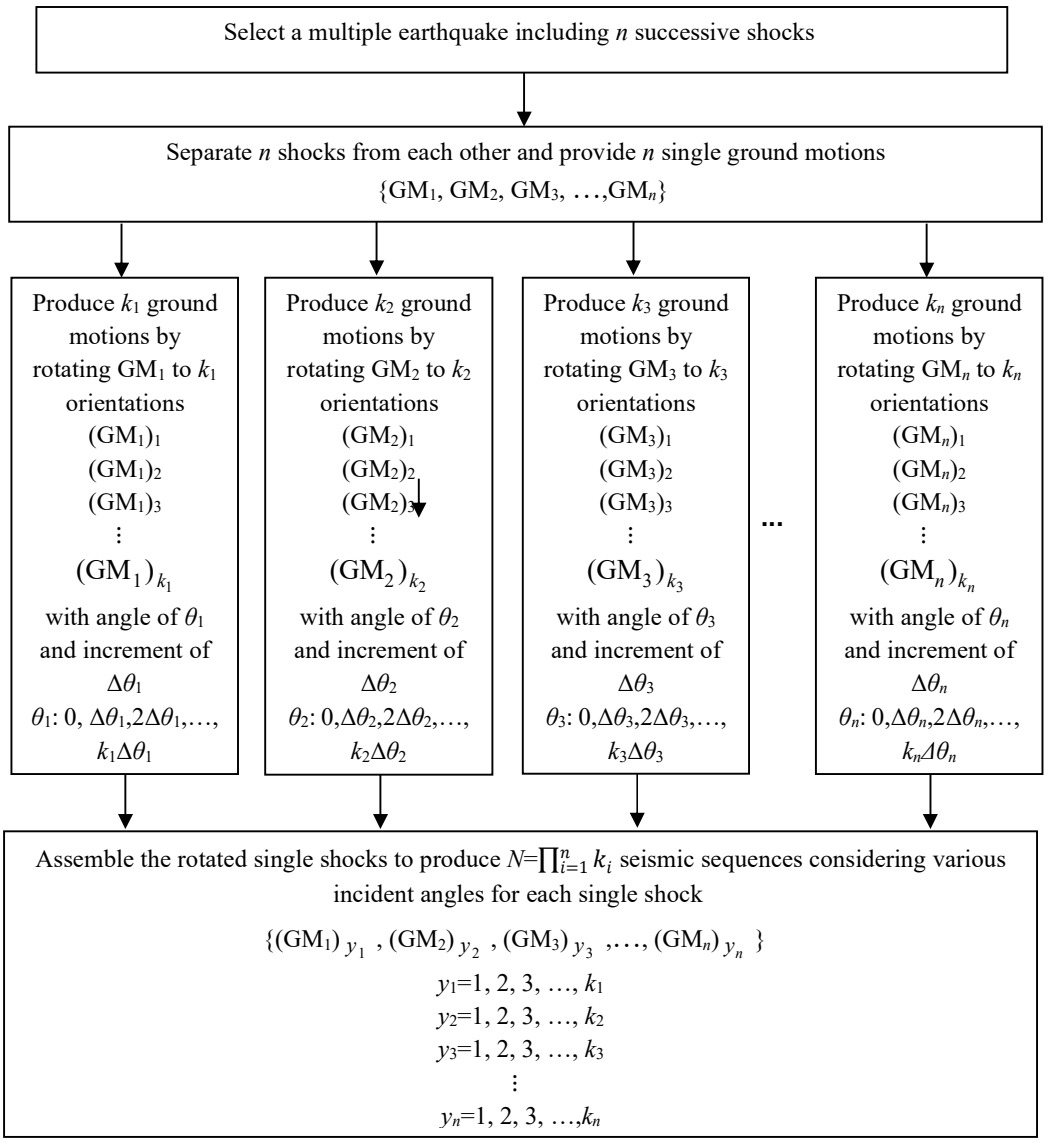

Fig. 1. Generation of rotated seismic sequences taken from [33]

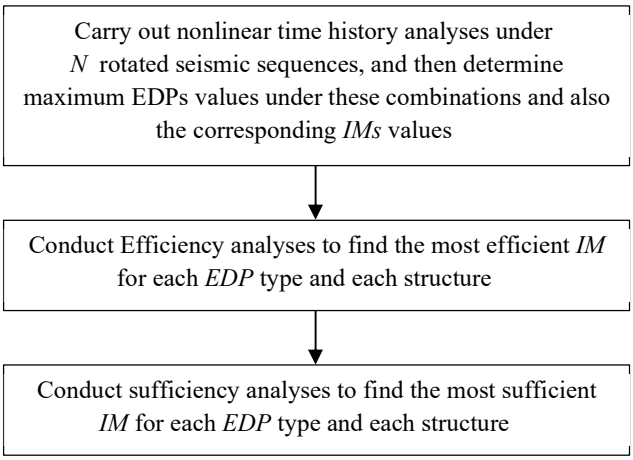

Fig. 2. Flowchart showing the required steps to find the most appropriate IM

In order to perform time history analyses under two horizontal components of earthquake, two orthogonal SDOF presented with 2D-SDOF is employed in this paper as the reference structural system. To model this system, two orthogonal elastic perfectly plastic springs are used. These springs are used to achieve the target fundamental vibration period (T), which is one of three values of 0.5, 1.0, and 2.0 sec for each orthogonal direction. The lateral strength of the system is quantified by the strength modification factor (R) using Eq. (1):

$$R = \frac{m S_a}{F_y} \tag{1}$$

where, m is the mass of the system, S_a denotes the spectral acceleration, and F_y stands for the lateral yield strength. This parameter is employed for both orthogonal directions with the values of 2.0, .0, and 6.0. In total, nine combinations of R and also nine combinations of T are selected for the directions, namely T_x, T_y= 0.5 sec, 1.0 sec, and 2.0 sec, and R_x, R_y=2.0, 4.0, and 6.0. Furthermore, the viscous damping ratio (ξ) is considered as a constant value of 5%.

3. Mainshock-aftershock sequences

In this study, 40 real mainshock-aftershock sequences are selected from the Pacific Earthquake Engineering Research (PEER) database [52]. The sequences including one mainshock and one subsequent aftershock are taken into account based on the following criteria as presented in [7]: (1) moment magnitude ($\boldsymbol{M_w}$) is not less than 5.0; (2) average horizontal Peak Ground Acceleration (PGA) is not less than 0.04 g; (3) average horizontal Peak Ground Velocity (PGV) is not less than 1.0 cm/sec; (4) closest site-to-fault-rupture distance is less than 75 km, and (5) average shear-wave velocity for the upper 30 m soil depth (V_{S30}), is within 100 and 1000 m/sec. The seismic sequences used in this study are shown in Table 1. It should be noted that preferences regarding the epicentral distance of the selected records are not considered. In addition, a 60-sec time gap with zero acceleration is considered between the mainshock and the subsequent aftershock in order to rest the structure after the first seismic

event. The distribution of the moment magnitude versus *PGA* and epicentral distance is shown in Fig. 3. 239 240

Table 1. Mainshock–aftershock sequences 241

Earthquake	Magnitude		Site	Significant duration (t_d) (Sec)		Epicentral distance (km)	
	Mainshock	Aftershock		Mainshock	Aftershock	Mainshock	Aftershock
Managua, Nicaragua (1972.12.23)	6.24	5.20	D	10.1	7.53	4.06	7.57
Imperial Valley (1979.10.15)	6.53	5.01	D	8.255	6.96	5.09	13.33
				6.685	6.4	3.95	13.86
				11.04	8.715	7.05	14.43
				9.665	12.265	10.45	15.19
				11.81	7.01	2.68	15.83
				8.7	5.11	7.65	12.45
				11.45	6.46	12.45	17.24
				6.95	7.055	1.35	13.16
				7.76	9.25	10.13	13.01
		5.62	D	24.67	11.315	15.25	20.53
Livermore (1980.01.24)	5.80	5.42	D	25.235	19.035	20.53	26.06
				10.31	5.605	20.92	22.02
Mammoth Lakes (1980.05.25)	6.06	5.69	D	9.18	7.425	6.63	9.46
Mammoth Lakes (1980.05.25)	5.91	5.70	D	7.305	4.535	19.71	15.04
Mammoth Lakes (1983.01.07)	5.34	5.31	D	7.19	7.115	9.40	10.76
Irpinia, Italy (1980.11.23)	6.90	6.20	C	19.5141	14.8161	8.18	19.56
				23.3376	19.0128	17.64	8.83
			D	26.6713	18.6586	29.8	44.41
				24.534	20.5262	30.07	22.69
Whittier Narrows (1987.10.01)	5.99	5.27	D	7.655	11.28	25.86	27.14
				9.255	12.22	20.82	20.98
				9.525	10.79	23.29	24.45
				13.59	10.79	25.94	27.8
				11.46	16.145	24.08	25.67
				8.005	5.25	15.18	15.19
			C	10.06	4.005	22.73	22.98
				11.415	3.63	15.94	14.84
				5.27	4.425	14.66	14.02
Northridge (1994.01.17)	6.69	5.28	D	12.98	9.52	8.66	13.51
				16.58	15.02	29.88	29.89
				12.02	7.38	24.03	23.99
				13.18	7.26	23.41	23.44
				8.78	9.14	26.45	27.82
				11.63	12.65	36.62	36.73

Earthquake	Magnitude		Site	Significant duration (t_d) (Sec)		Epicentral distance (km)	
	Mainshock	Aftershock		Mainshock	Aftershock	Mainshock	Aftershock
		5.93	C	9.08	8.56	20.72	28.69
Kocaeli & Duzce, Turkey (1999.08.17)	7.51	7.14	D	11.79	10.945	15.37	6.58
Chi-Chi, Taiwan (1999.09.20)	7.62	6.20	D	44.275	29.02	59.8	67.91
		6.30	C	41.805 27.204	38.165 10.48	34.18 42.16	59.98 70.37

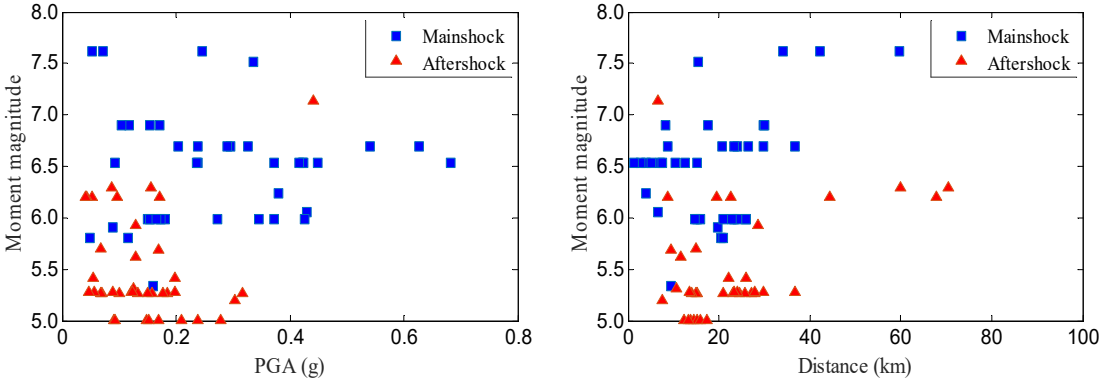

(a) (b)

Fig. 3. The characteristics of mainshocks and aftershocks: (a). Moment magnitude–*PGA* distribution; (b). Moment magnitude–distance distribution

3. Intensity Measures (*IMs*) and Engineering Demand Parameters (*EDPs*)

In this paper, the correlation between a large number of ground motion IM*s*, including non-spectral and cumulative-based ones and four *EDPs* is investigated. Peak-based *IMs*, such as *PGA*, cannot be always used as efficient measures of earthquake in the case of multiple ground motions. Hence, the selection of *IMs* is performed based on the cumulative-based and non-spectral *IMs*, such that the appropriate choice of the peak-based *IM* between mainshock, aftershock, and sequence, or their combination as a unique *IM* would not be a challenging effort. Table 2 indicates 15 *IMs* employed in this study.

Moreover, four *EDPs* including (a) maximum inelastic displacement, *MD*, which is a broadly accepted seismic response in practice; (b) maximum inelastic absolute acceleration, *MA*, as an appropriate indicator to investigate nonstructural elements; (c) residual displacement, *RD*, which can be a significant measure of structural inelasticity; and (d) hysteretic energy, *EH*, as an effective proxy of cumulative structural damage.

Table 2. Non-spectral and cumulative-based Intensity Measures

N.O.	Intensity Measure (*IM*)	Definition
1	Squared acceleration	$a_{\text{sq}} = E_a = \int_0^{t_f} a(t)^2\,dt$
2	Squared velocity Specific Energy Density [53]	$SED = v_{\text{sq}} = E_v = \int_0^{t_f} v(t)^2\,dt$
3	Squared displacement	$d_{\text{sq}} = E_d = \int_0^{t_f} d(t)^2\,dt$
4	Root square acceleration [54]	$a_{\text{rs}} = \sqrt{a_{sq}}$
5	Root square velocity	$v_{\text{rs}} = \sqrt{v_{sq}}$
6	Root square displacement	$d_{\text{rs}} = \sqrt{d_{sq}}$
7	Arias intensity [55]	$I_A = \frac{\pi}{2g}\int_0^{t_f} a(t)^2\,dt$
8	Significant duration [56]	$t_d = t(0.95I_A) - t(0.05I_A)$
9	Cumulative Absolute Velocity [57]	$CAV = \int_0^{t_f} \lvert a(t)\rvert dt$
10	Cumulative Absolute Displacement [58]	$CAD = \int_0^{t_f} \lvert v(t)\rvert dt$
11	Cumulative Absolute Impulse	$CAI = \int_0^{t_f} \lvert d(t)\rvert dt$
12	Root-Mean-Square (rms) of acceleration [59]	$a_{\text{rms}} = \sqrt{\frac{1}{t_d}\int_0^{t_f} a(t)^2\,dt}$
13	Root-Mean-Square (rms) of velocity [59]	$v_{\text{rms}} = \sqrt{\frac{1}{t_d}\int_0^{t_f} v(t)^2\,dt}$
14	Root-Mean-Square (rms) of displacement [59]	$d_{\text{rms}} = \sqrt{\frac{1}{t_d}\int_0^{t_f} d(t)^2\,dt}$
15	Characteristic intensity [60]	$I_c = {a_{\text{rms}}}^{1.5}(t_d)^{0.5}$

4. Efficiency

Ground motion intensity measure (IM) is defined as an efficient IM, if it is capable of resulting in a reduced variability in the seismic demands of structures for a given value of IM. In order to determine the best IM predicting the considered EDP*s*, the correlation coefficient of regression is applied. If the Pearson correlation coefficient would be a relatively high value, a higher efficiency is obtained. The simple model shown in the following equation is employed for the regression analysis [61]:

$$EDP = a\, IM^{\,b} \tag{2}$$

where a and b are the regression coefficients. In logarithmic space, Equation (2) is as:

$$\ln(EDP) = b \ln(IM) + \ln(a) + e \tag{3}$$

in which, e stands for a zero-mean random variable that shows the variability of ln(EDP) given the IM. It should be noted that the results presented in this study are based on the 2D-SDOF systems with modelling simplification. Complicated systems with more degrees of freedom are needed to extend the results.

Figure 4 indicates the Pearson correlation coefficient (ρ) between the 15 ground motion IMs and the maximum displacement (MD) of regular systems (T_x=T_y=T and R_x=R_y=R) with the variety of T and R values. As shown in this figure, the value of ρ between SED and MD of T_x=T_y=0.5 sec and R_x=R_y=6 is 0.956, between v_{rms}, and MD of T_x=T_y=1.0 sec and R_x=R_y=6 is 0.950, and between d_{rms} and MD of T_x=T_y=0.5 sec and R_x=R_y=6 is 0.953. This demonstrates that these IMs have higher efficiency compared with the other ones in the case of MD of the regular structures under mainshock-aftershock sequences, depending on the values of T and R.

Figure 5 represents the ρ values between the considered IMs and the four EDPs of regular (T_x=T_y and R_x=R_y). Also, the efficiency of the 15 IMs is indicated based on the Pearson correlation coefficient for irregular structures (T_x≠T_y or R_x≠R_y) in Figs. 6 and 7.

It can be concluded from Fig. 5(a), namely the structures with Rx=Ry=2, Tx=Ty=0.5 sec, that for the vast majority of the IMs (14 out of 15), the correlation with the *MD* demand is stronger compared to the other demands. While in Fig. 5(b) and (c), the values of ρ for the majority of the IMs are higher when *EH* is considered as the response parameter. It shows that for the short-period regular structural systems with low strength reduction factor, more IMs considered are expected to be correlated well with *MD* ($\rho > 0.7$), whereas for the moderate-to-long period regular systems, the most appropriate demand quantity is *EH*. This is also observed for irregular structures ($T_x \neq T_y$ or $R_x \neq R_y$) according to Figs. 6 and 7, such that *EH* is correlated efficiently with more IMs, compared to the other given EDPs.

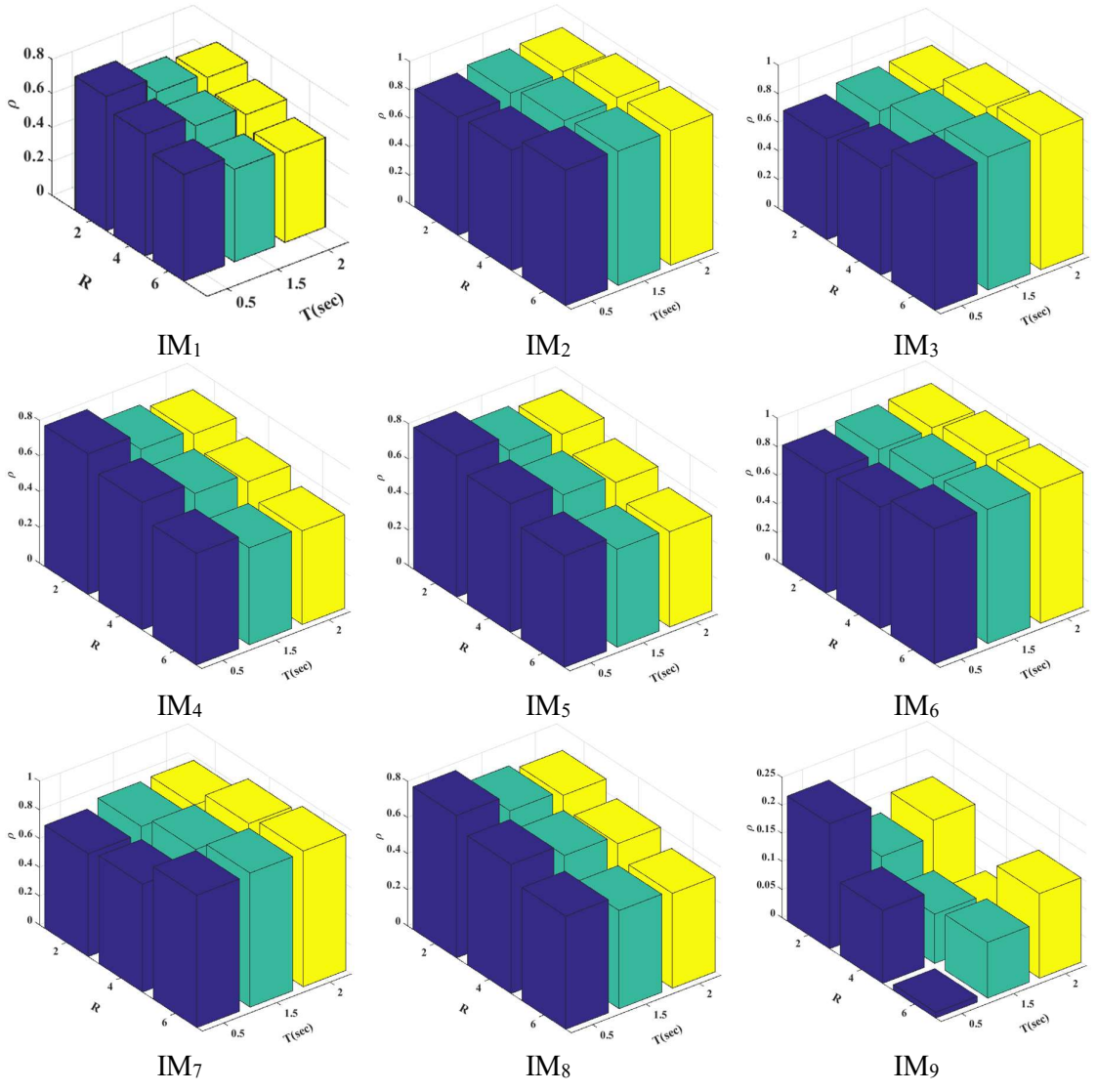

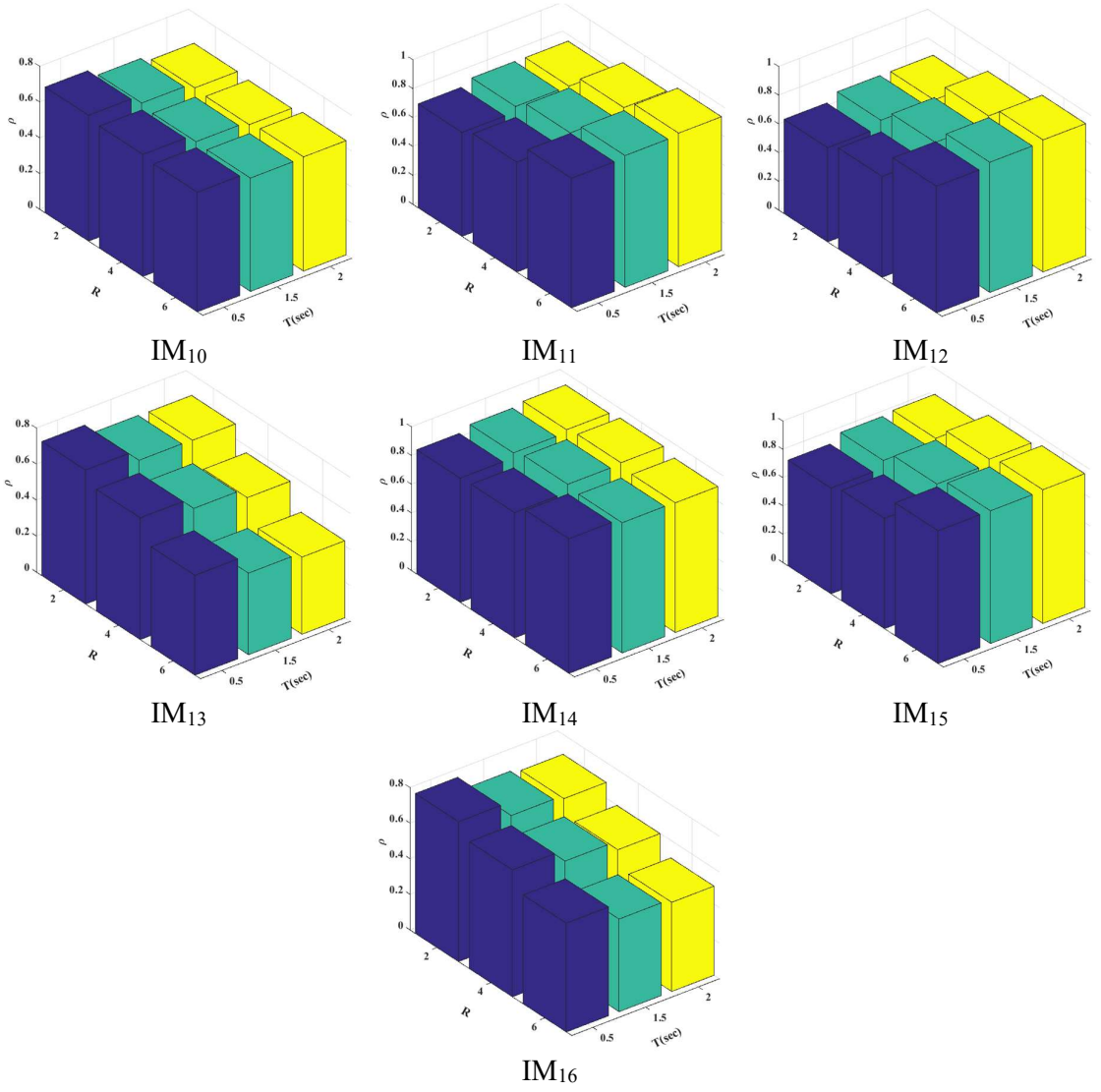

Fig. 4. The Pearson correlation coefficient (ρ) between the 15 ground motion IMs and the maximum displacement of regular systems

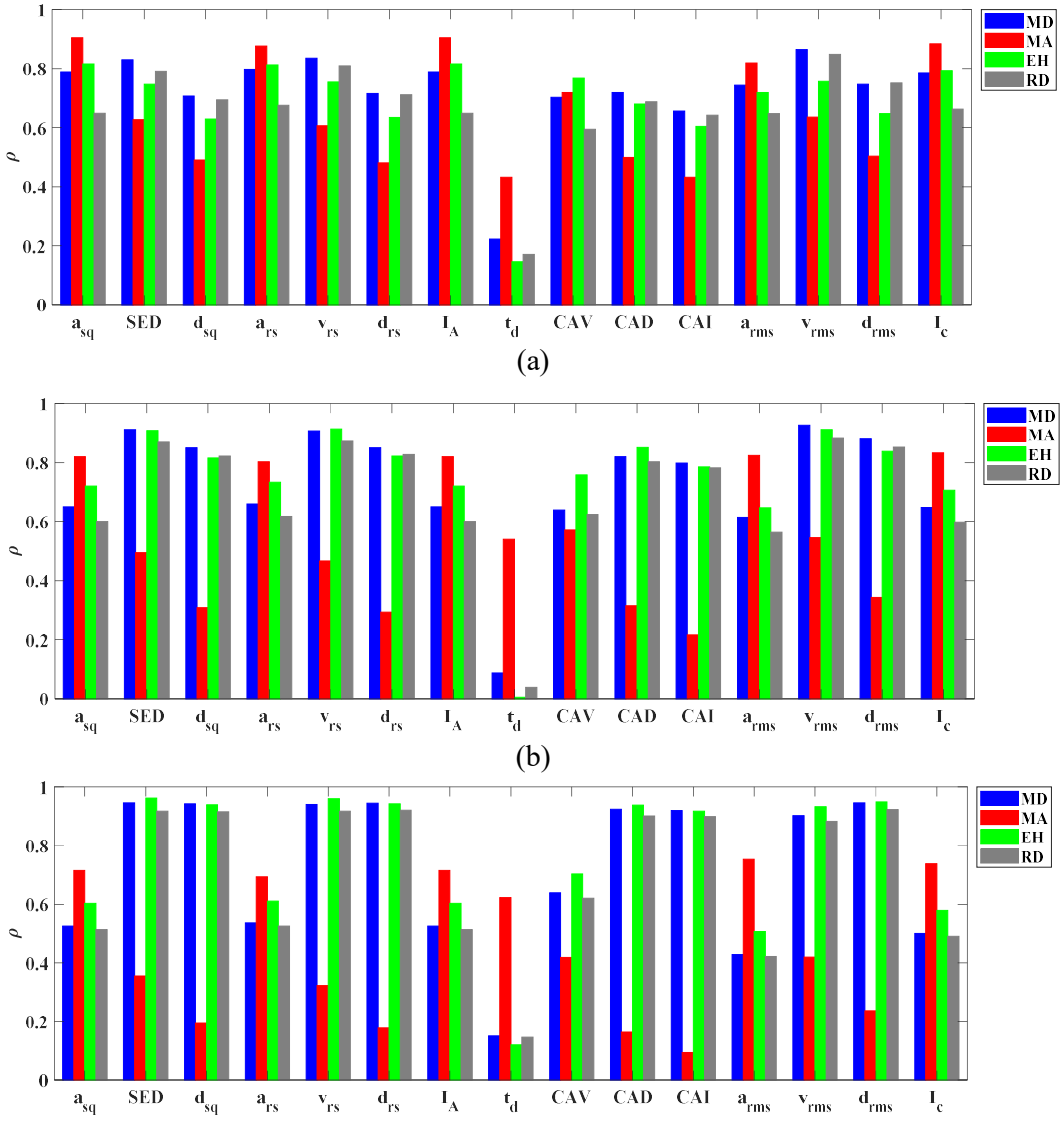

Fig. 5. The Pearson correlation coefficient (ρ) between the 15 earthquake IMs and the four EDPs of regular systems (T_x=T_y or R_x=R_y): (a) *Rx*=*Ry*=2, *Tx*=*Ty*=0.5 sec; (b) *Rx*=*Ry*=4, T_X=*Ty*=1.0 sec; (c) *Rx*=*Ry*=6, T_X=*Ty*=2.0 sec

297

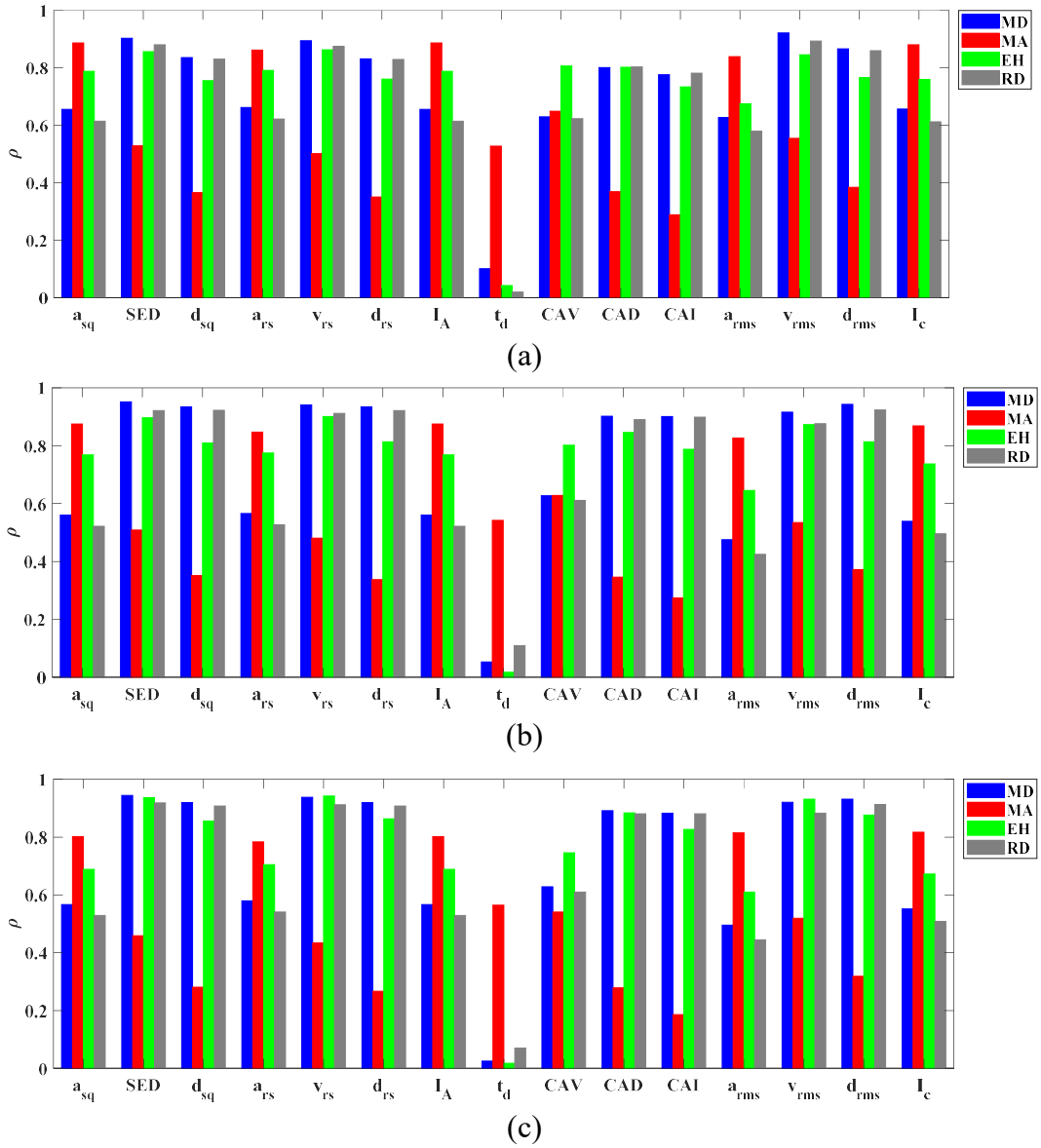

Fig. 6. The Pearson correlation coefficient (ρ) between the 15 ground motion IMs and the four EDPs of irregular systems (T_x=T_y or R_x≠R_y): (a) *Rx*=2, *Ry*=4, *Tx*=*Ty*=1.0 sec; (b) *Rx*=2, *Ry*=6, *Tx*=*Ty*=1.0 sec; (c) *Rx*=4, *Ry*=6, *Tx*=*Ty*=1.0 sec

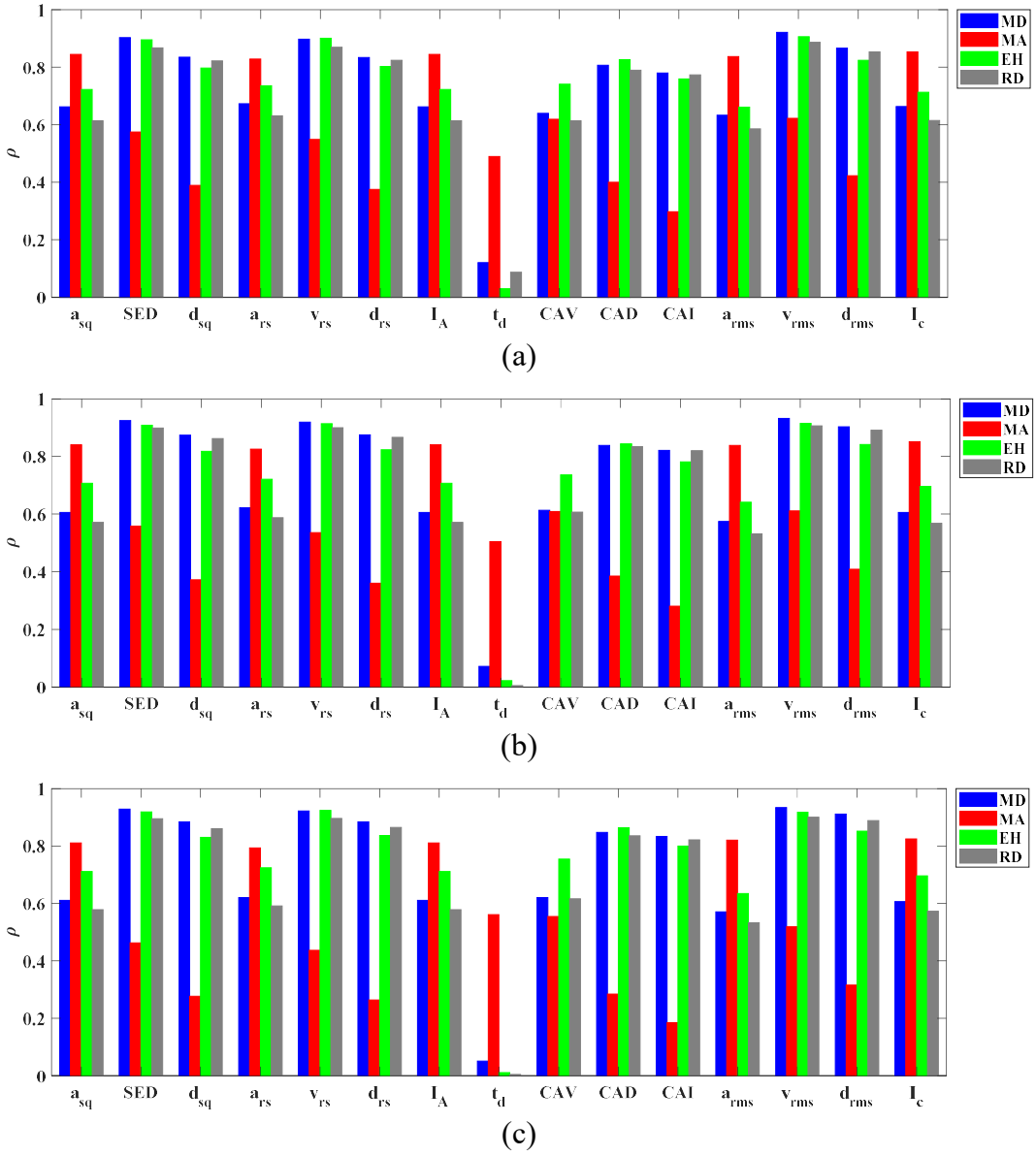

Fig. 7. The Pearson correlation coefficient (ρ) between the 15 ground motion IMs and the four EDPs of irregular systems ($T_x \neq T_y$ or $R_x = R_y$): (a) Rx=Ry=4, Tx=0.5 sec, Ty=1.0 sec; (b) Rx=4, Ry=4, Tx=0.5 sec, Ty=2.0 sec; (c) Rx=Ry=4, Tx=1.0 sec, Ty=2.0 sec

Table 3 shows the efficient IMs for different EDPs of the regular and irregular systems. Considering the values of ρ for three IMs are high and close to each other, Table 3 indicates three efficient IMs for various EDPs of the regular and irregular structures. As concluded from the table, v_{rms}, v_{sq}, v_{rs} are generally the most efficient IMs.

Figure 8 indicates the histogram of the candidate IMs, stated in Table 3, for all seismic sequences considered (121×40 records). This figure demonstrates that three ranges can be considered for the IMs. The appropriate range for a_{sq}, v_{rs}, and I_c are concluded in the first half of their ranges. While this range is in the first third of their variety of v_{sq} and v_{rms}. Also, the relatively uniform distribution is observed for a_{rms}, such that it selection is not dependent on the selected range. As a result, a_{rms} can be the most reliable IM among the candidate IMs considering the structures and seismic sequences examined in this study.

Table 3. The candidate efficient non-spectral and cumulative-based Intensity Measures for regular and irregular structures

Regular		Irregular	
EDP	IMs	EDP	IMs
MD	v_{rms} v_{sq} v_{rs}	*MD*	v_{sq} v_{rms} v_{rs}
MA	I_c a_{rms} a_{sq}	*MA*	I_c a_{rms} a_{sq}
EH	v_{rs} v_{sq} v_{rms}	*EH*	v_{rs} v_{sq} v_{rms}
RD	v_{rms} v_{rs} v_{sq}	*RD*	v_{sq} v_{rs} v_{rms}

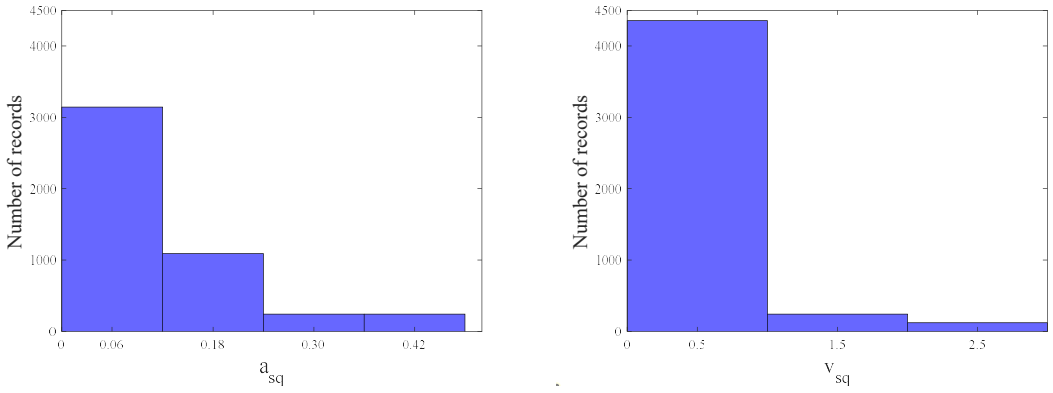

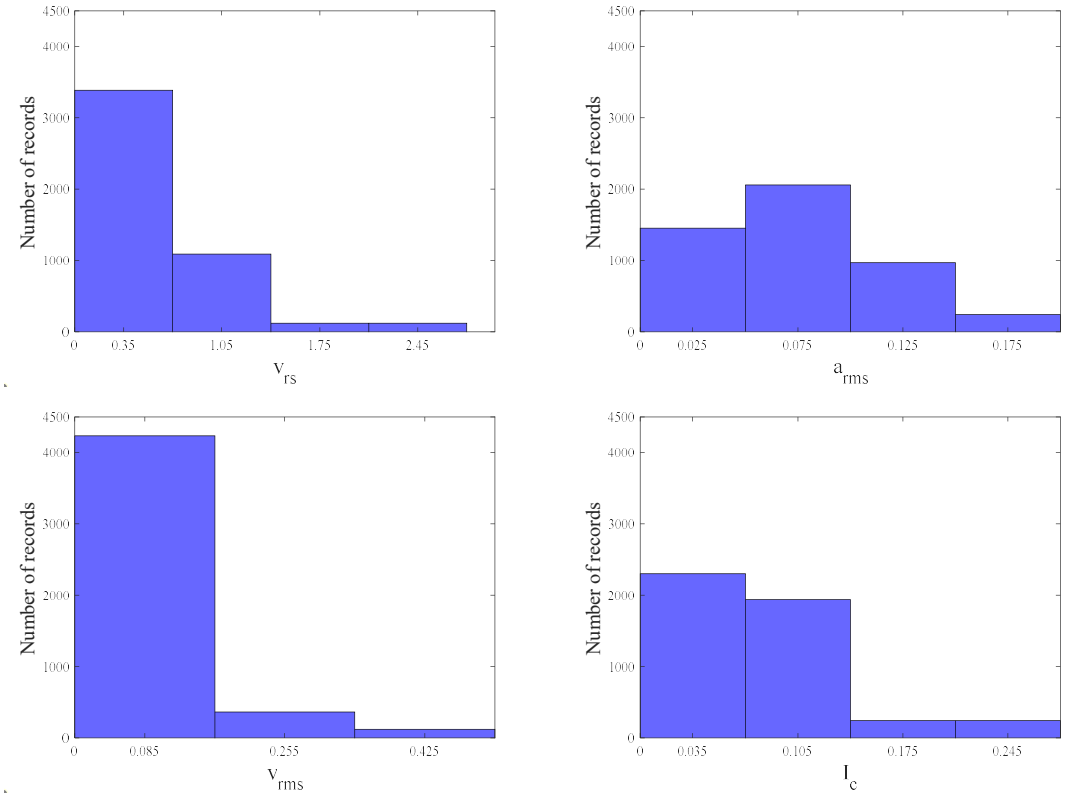

Fig. 8. Histogram of the candidate IMs

5. Sufficiency

A ground motion intensity is sufficient, if it would be independent of any other seismological parameter, particularly the earthquake magnitude and the epicenteral distance [51]. The sufficiency property of the IM is determined using regression analyses on the residuals of the *EDP*, EDP_{res}, relative to the magnitude (M) and also the epicentral distance (R) of the seismic sequences, including both mainshock and aftershock, which is shown as $EDP_{res}|IM$. Since the magnitude and epicentral distance of mainshock and subsequent aftershock can be different to each other, four investigations are performed to assess the efficiency of IMs relative to the magnitude and epicentral distance of both mainshock and aftershock. In this regard, the magnitude and epicentral distance of mainshocks are indicated by *MM* and *RM* respectively. Similarly, the characteristics related to aftershocks are shown by *MA* and *RA* respectively. In General, $EDP_{res}|IM$ is defined as the differences between the EDP computed from numerical analyses and that calculated using the regression fit line, which the

latter is obtained from the efficiency process of the IM. Therefore, the sufficiency is quantified by computing the relevant p-values from the regressions of $EDP_{res}|IM$ relative to the seismological characteristics (M and R) of the sequential earthquakes selected in this study. A cut-off p-value of 0.05 is considered to differentiate between sufficient and insufficient ground motions IMs [51].

Figs 8-11 illustrate the computed *p-value* for the 15 ground motion IMs and the four EDPs of both regular and irregular structures through regression analyses of $EDP_{res}|IM$ relative to M and R of the selected multiple ground motions. It is observed from these figures that the *p-value* for most of the IMs and most of the regular structures is more than 0.05 in the case of *MD*, *EH* and *RD*. However, when *MA* of the regular systems is considered as the seismic response, the *p-value* is less than 5% for IM_7 to IM_{15}. Moreover, the sufficiency for most of the IMs and *EH* and *RD* of most of the irregular structures is high (*p-value* > 0.05). Additionally, in the case of *MD* and *MA* of the irregular structures, *p-value* lower than 0.05 is attributed to IM_7 to IM_{15}. In general, if the *MD*, *MA*, *EH* and *RD* of the regular systems are taken into account as the demand parameters, the optimal IMs in terms of efficiency and sufficiency are IM_2, IM_{12}, IM_5 and IM_2, respectively.

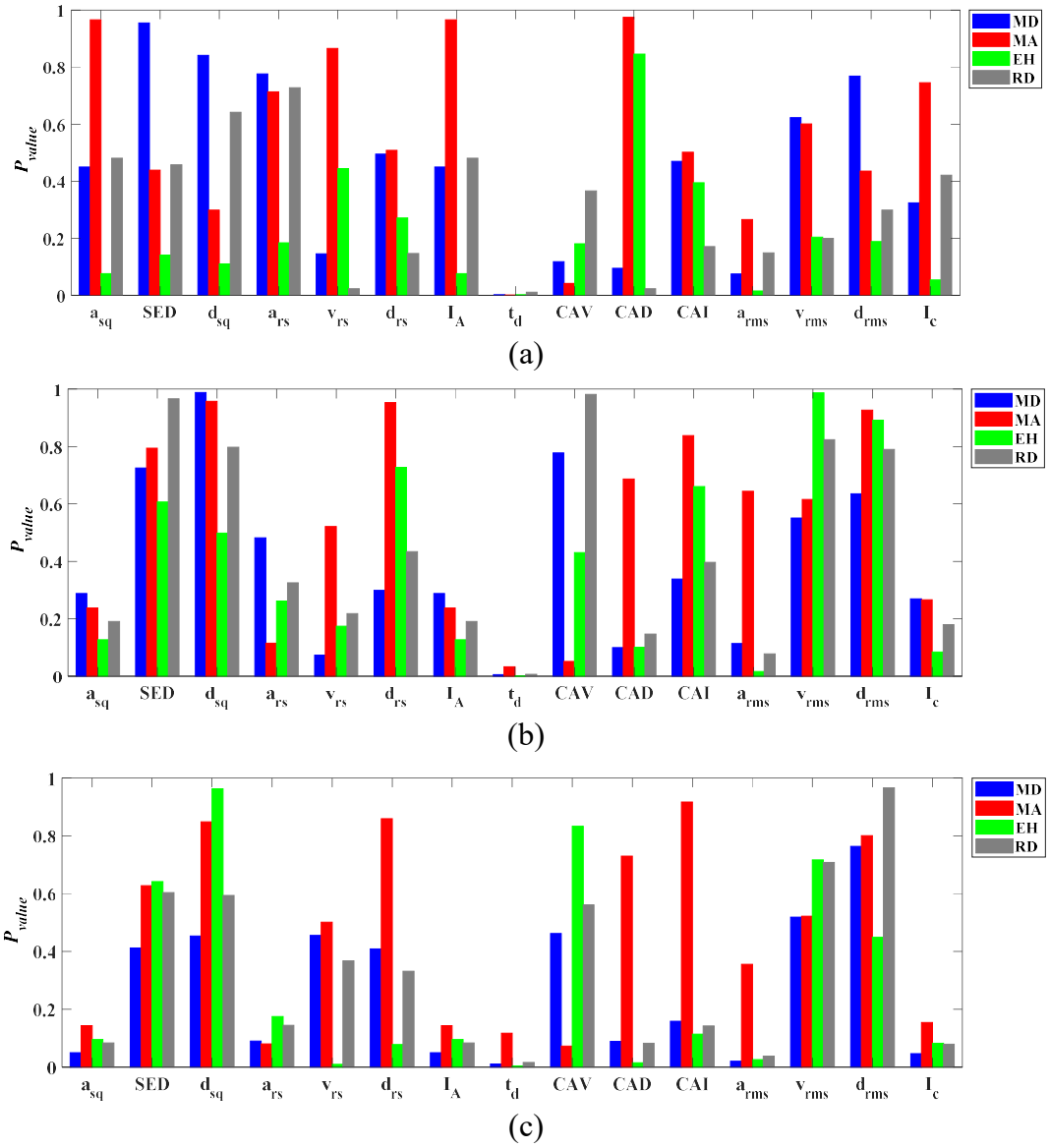

Fig. 8. *p-value* for regular systems (T_x=T_y or R_x=R_y): (a) *Rx*=*Ry*=2, *Tx*=*Ty*=0.5 sec; (b) *Rx*=*Ry*=4, T_X=*Ty*=1.0 sec; (c) *Rx*=*Ry*=6, T_X=*Ty*=2.0 sec through regression analyses of $EDP_{res}|IM$ relative to the magnitudes (M) of mainshocks

348

349

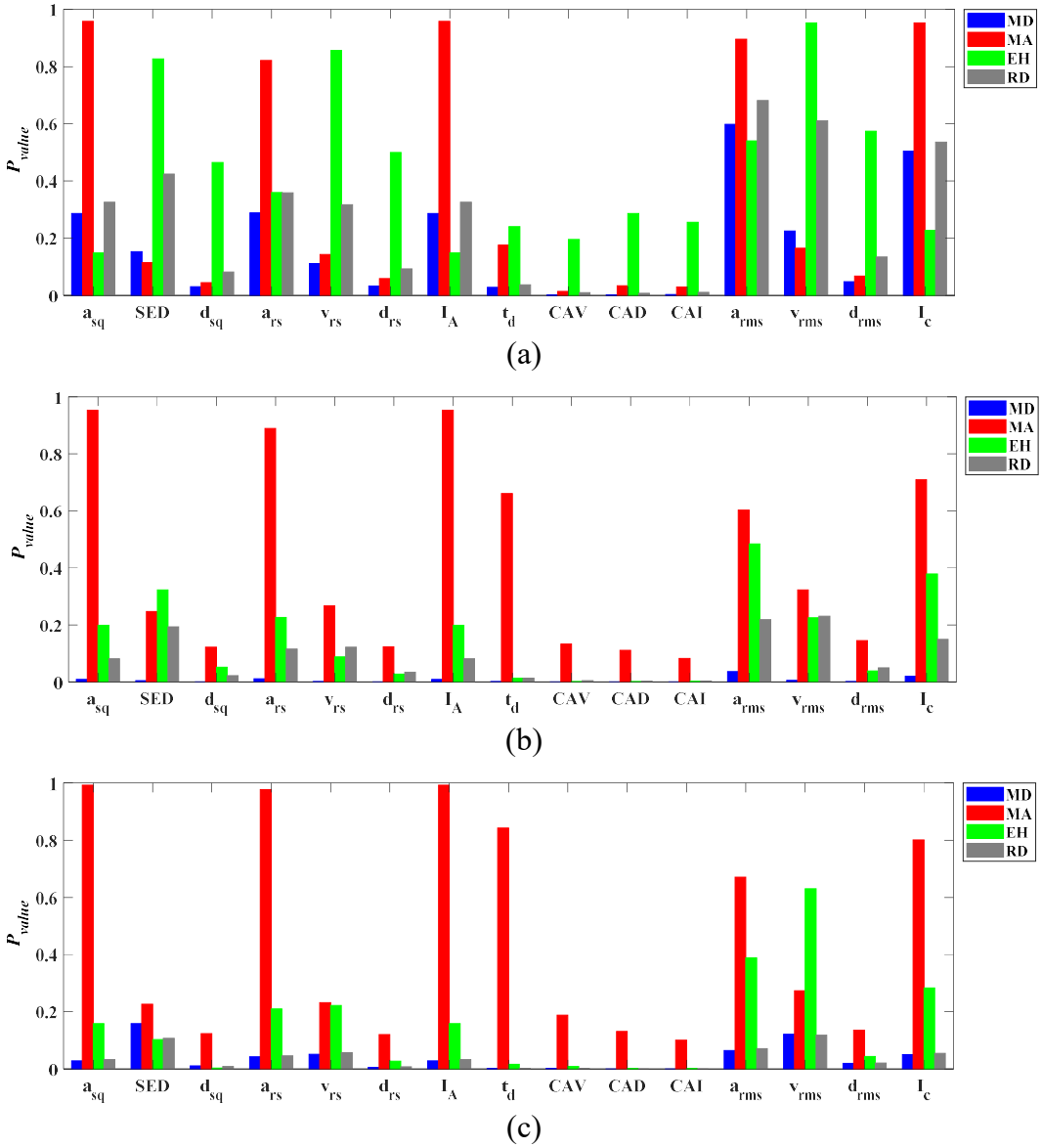

Fig. 9. *p-value* for regular systems (T_x=T_y or R_x=R_y): (a) *Rx*=*Ry*=2, *Tx*=*Ty*=0.5 sec; (b) *Rx*=*Ry*=4, T_X=*Ty*=1.0 sec; (c) *Rx*=*Ry*=6, T_X=*Ty*=2.0 sec through regression analyses of $EDP_{res}|IM$ relative to the epicentral distance of mainshocks

350

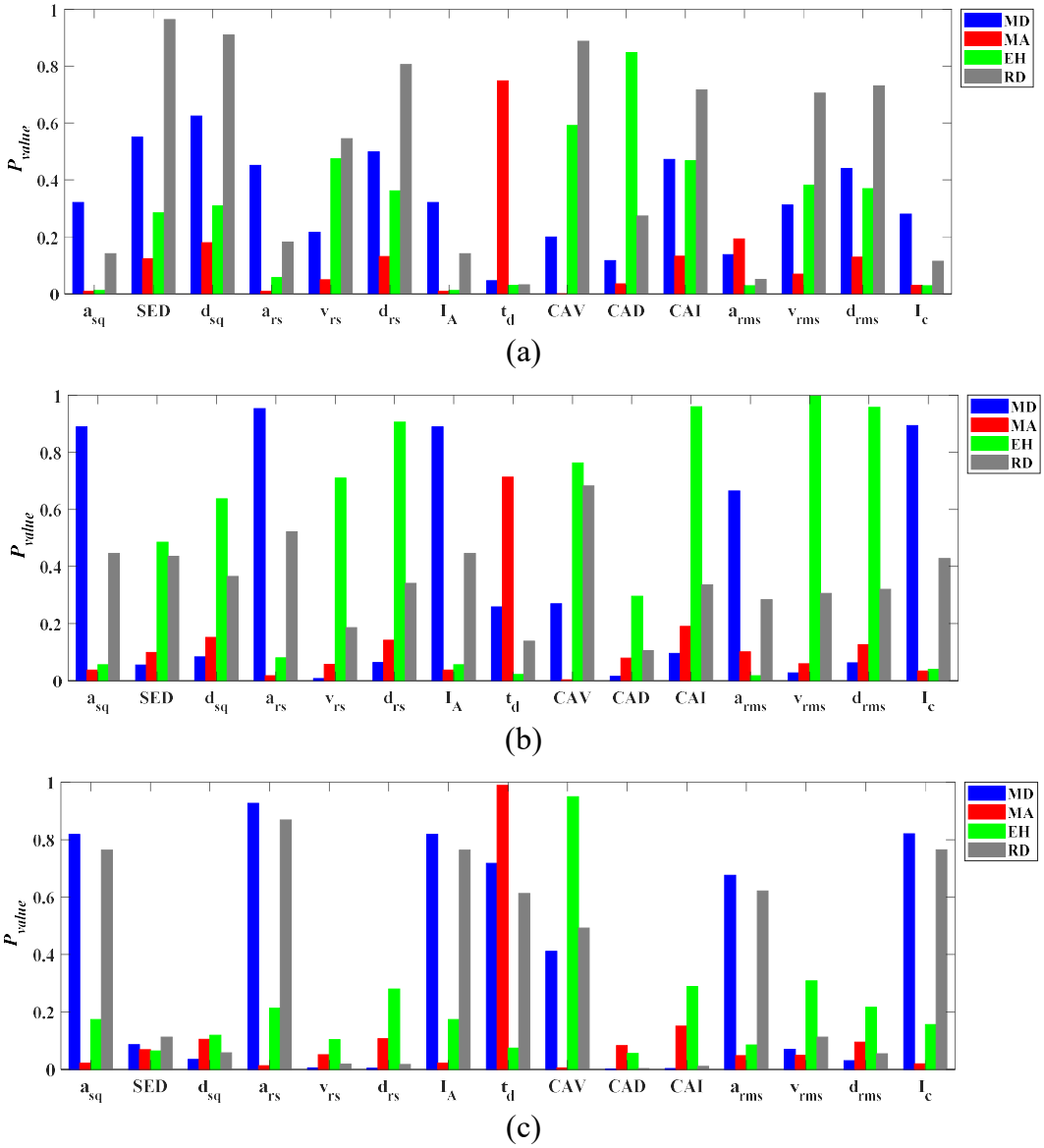

Fig. 10. *p-value* for regular systems (T_x=T_y or R_x=R_y): (a) *Rx*=*Ry*=2, *Tx*=*Ty*=0.5 sec; (b) *Rx*=*Ry*=4, T_X=*Ty*=1.0 sec; (c) *Rx*=*Ry*=6, T_X=*Ty*=2.0 sec through regression analyses of $EDP_{res}|IM$ relative to the magnitudes (M) of aftershocks

351

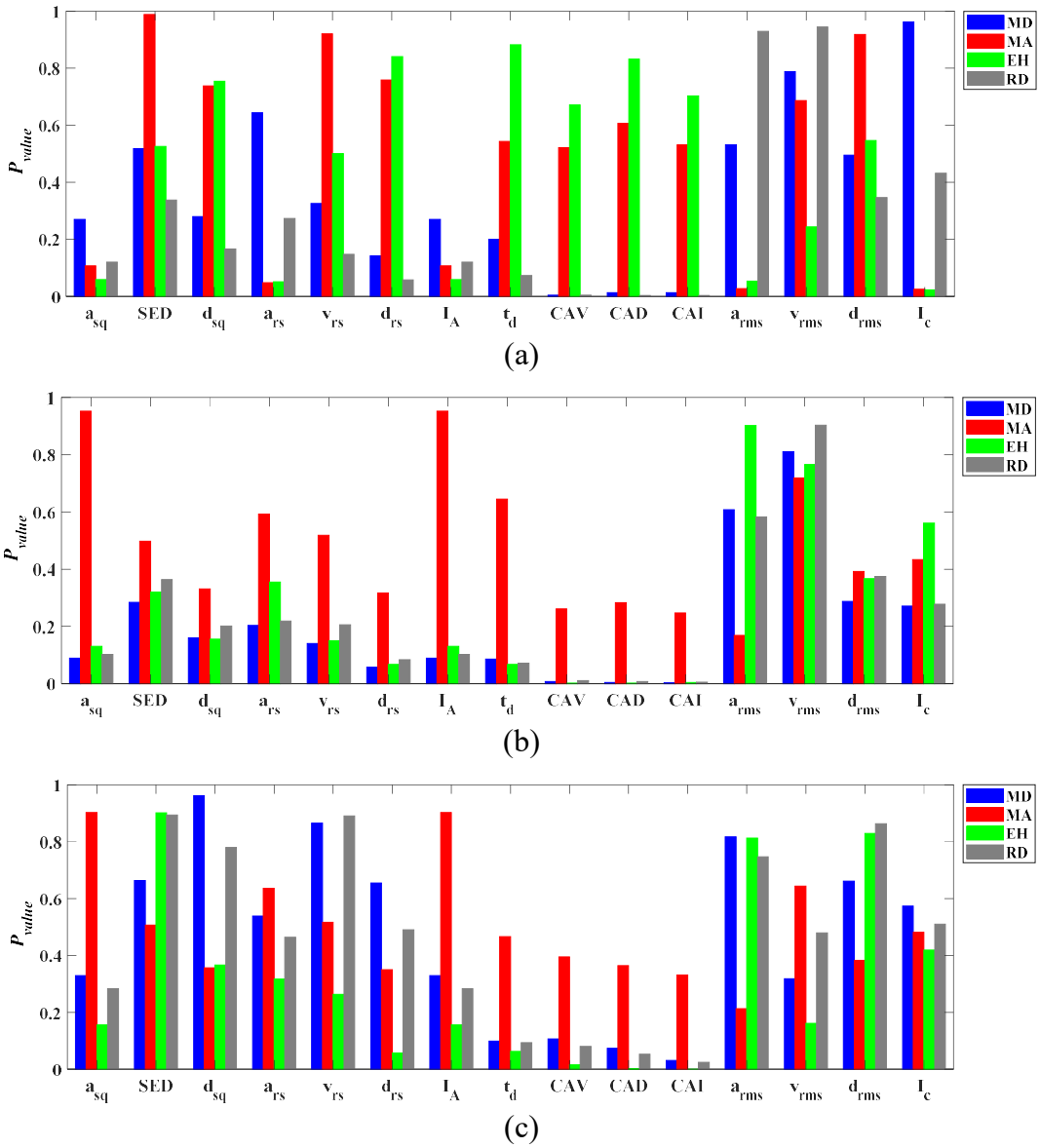

Fig. 11. *p-value* for regular systems (T_x=T_y or R_x=R_y): (a) *Rx*=*Ry*=2, *Tx*=*Ty*=0.5 sec; (b) *Rx*=*Ry*=4, T_X=*Ty*=1.0 sec; (c) *Rx*=*Ry*=6, T_X=*Ty*=2.0 sec through regression analyses of $EDP_{res}|IM$ relative to the epicentral distance of aftershocks

6. Summary and conclusions

This study investigates the correlation between 15 non-spectral and cumulative-based ground motion IM*s* and the four *EDPs* of the structures characterized by 2D-SDOF systems under multiple ground motions in terms of the efficiency and sufficiency considering a wide variety of incident angle. In this regard, the relative difference between directions of mainshocks and subsequent aftershocks is considered. These angels can come from the same seismic source

and therefore, the results presented in this article should be analyzed by considering certain level of correlation between both angles. Considering the multiple incident angle, a large number of repeated seismic sequences are generated as the input excitation of nonlinear dynamic analysis of the systems. It is concluded from the extensive parametric analyses carried out in the paper that v_{sq}, v_{rms}, and d_{rms} have higher efficiency in comparison with the other selected IMs in the case of *MD* of the regular structures subjected to multiple earthquakes. Correlation between the vast majority of the IMs (14 out of 15) and the *MD* of these systems is stronger compared to the other demands, namely *MA*, *EH*, and *RD*. However, higher values of ρ are obtained for the majority of the IMs in the case of *EH* of the same structures. In addition, for the short-period regular systems with low strength reduction factor, more IMs correlate well with *MD* ($\rho > 0.7$), while for moderate-to-long period regular systems, the most appropriate EDP is *EH*. Also, for irregular structures, the correlation between more IM and *EH* is high. Generally, three candidate IMs in terms of the efficiency are v_{rms}, v_{sq}, and v_{rs} for *MD*, *EH*, and *RD*, whereas for *MA* the efficient IMs are I_c, a_{rms}, and a_{sq}. Furthermore, when the *MD*, *MA*, *EH* and *RD* of the regular systems are considered as the seismic demands, the optimal IMs in terms of efficiency and sufficiency are v_{sq}, a_{rms}, v_{rs} and v_{sq}, respectively.

References

[1] RMS. “Reconnaissance report: The 2008 wenchuan earthquake: Risk management lessons and implications.” Risk Management Solutions, Newark, CA, U.S., 2008, https://forms2.rms.com/rs/729-DJX-565/images/eq_2008_wenchuaneq.pdf, in.

[2] M. Kazama, T. Noda, Damage statistics (Summary of the 2011 off the Pacific Coast of Tohoku Earthquake damage), Soils and Foundations, 52 (2012) 780-792.

[3] F.F. Pollitz, R.S. Stein, V. Sevilgen, R. Bürgmann, The 11 April 2012 east Indian Ocean earthquake triggered large aftershocks worldwide, Nature, 490 (2012) 250-253.

[4] M.G. Durante, L. Di Sarno, P. Zimmaro, J.P. Stewart, Damage to roadway infrastructure from 2016 Central Italy earthquake sequence, Earthquake spectra, 34 (2018) 1721-1737.

[5] D. Samadian, M. Eghbali, M. Raissi Dehkordi, M. Ghafory-Ashtiany, Recovery and reconstruction of schools after M 7.3 Ezgeleh-Sarpole-Zahab earthquake of Nov. 2017; part I: Structural and nonstructural damages after the earthquake, Soil Dynamics and Earthquake Engineering, 139 (2020) 106305.

[6] https://www.usgs.gov/news/magnitude-72-earthquake-haiti, in.

[7] K. Goda, C.A. Taylor, Effects of aftershocks on peak ductility demand due to strong ground motion records from shallow crustal earthquakes, Earthquake Engineering & Structural Dynamics, 41 (2012) 2311-2330.

[8] W. Wen, C. Zhai, D. Ji, Damage spectra of global crustal seismic sequences considering scaling issues of aftershock ground motions, Earthquake Engineering & Structural Dynamics, 47 (2018) 2076-2093.

[9] S. Amiri, E. Bojórquez, Residual displacement ratios of structures under mainshock-aftershock sequences, Soil Dynamics and Earthquake Engineering, 121 (2019) 179-193.

[10] L. Di Sarno, S. Amiri, Period elongation of deteriorating structures under mainshock-aftershock sequences, Engineering Structures, 196 (2019) 109341.

[11] S. Amiri, A. Garakaninezhad, E. Bojórquez, Normalized residual displacement spectra for post-mainshock assessment of structures subjected to aftershocks, Earthquake Engineering and Engineering Vibration, 20 (2021) 403-421.

[12] M. Raghunandan, A.B. Liel, N. Luco, Aftershock collapse vulnerability assessment of reinforced concrete frame structures, Earthquake Engineering & Structural Dynamics, 44 (2015) 419-439.

[13] M. Shokrabadi, H.V. Burton, Risk-based assessment of aftershock and mainshock-aftershock seismic performance of reinforced concrete frames, Structural Safety, 73 (2018) 64-74.

[14] L. Di Sarno, F. Pugliese, Effects of mainshock-aftershock sequences on fragility analysis of RC buildings with ageing, Engineering Structures, 232 (2021) 111837.

[15] L. Di Sarno, J.-R. Wu, Fragility assessment of existing low-rise steel moment-resisting frames with masonry infills under mainshock-aftershock earthquake sequences, Bulletin of Earthquake Engineering, 19 (2021) 2483-2504.

[16] M. Kalateh-Ahani, S. Amiri, A Park-Ang damage index-based framework for post-mainshock structural safety assessment, Structures, 33 (2021) 820-829.

[17] M.C. Basim, F. Pourreza, M. Mousazadeh, A.A. Hamed, The effects of modeling uncertainties on the residual drift of steel structures under mainshock-aftershock sequences, in: Structures, Elsevier, 2022, pp. 912-926.

[18] H. Shafaei, H. Naderpour, Seismic fragility evaluation of FRP-retrofitted RC frames subjected to mainshock-aftershock records, in: Structures, Elsevier, 2020, pp. 950-961.

[19] K. Goda, Comparison of peak ductility demand of inelastic SDOF systems in maximum elastic response and major principal directions, Earthquake Spectra, 28 (2012) 385-399.

[20] M. Torbol, M. Shinozuka, The directionality effect in the seismic risk assessment of highway networks, Structure and Infrastructure Engineering, 10 (2014) 175-188.

[21] O. Taskari, A. Sextos, Multi-angle, multi-damage fragility curves for seismic assessment of bridges, Earthquake Engineering & Structural Dynamics, 44 (2015) 2281-2301.

[22] D. Giannopoulos, D. Vamvatsikos, Ground motion records for seismic performance assessment: To rotate or not to rotate?, Earthquake Engineering & Structural Dynamics, 47 (2018) 2410-2425.

[23] K.G. Kostinakis, G.E. Manoukas, A.M. Athanatopoulou, Influence of seismic incident angle on response of symmetric in plan buildings, KSCE Journal of Civil Engineering, 22 (2018) 725-735.

[24] Y. Wang, L. Ibarra, C. Pantelides, Effect of incidence angle on the seismic performance of skewed bridges retrofitted with buckling-restrained braces, Engineering Structures, 211 (2020) 110411.

[25] Z. Alam, C. Zhang, B. Samali, Influence of seismic incident angle on response uncertainty and structural performance of tall asymmetric structure, The Structural Design of Tall and Special Buildings, 29 (2020) e1750.

[26] B. Wei, Z. Hu, C. Zuo, W. Wang, L. Jiang, Effects of horizontal ground motion incident angle on the seismic risk assessment of a high-speed railway continuous bridge, Archives of Civil and Mechanical Engineering, 21 (2021) 18.

[27] J. Gong, X. Zhi, F. Fan, S. Shen, D. Qaio, J. Zhong, Effects of Seismic Incident Directionality on Ground Motion Characteristics and Responses of a Single-Mass Bi-Degree-of-Freedom System, International Journal of Structural Stability and Dynamics, 0 2150119.

[28] M. Yazdani, V. Jahangiri, Intensity measure-based probabilistic seismic evaluation and vulnerability assessment of ageing bridges, Earthquakes and Structures, 19 (2020) 379-393.

[29] M. Hatzivassiliou, G.D. Hatzigeorgiou, Seismic sequence effects on three-dimensional reinforced concrete buildings, Soil Dynamics and Earthquake Engineering, 72 (2015) 77-88.

[30] F. Hosseinpour, A.E. Abdelnaby, Fragility curves for RC frames under multiple earthquakes, Soil Dynamics and Earthquake Engineering, 98 (2017) 222-234.

[31] K. Kostinakis, K. Morfidis, The impact of successive earthquakes on the seismic damage of multistorey 3D R/C buildings, Earthquakes and Structures, 12 (2017) 1-12.

[32] E. Omranian, A.E. Abdelnaby, G. Abdollahzadeh, Seismic vulnerability assessment of RC skew bridges subjected to mainshock-aftershock sequences, Soil Dynamics and Earthquake Engineering, 114 (2018) 186-197.

[33] J. Ruiz-García, S. Yaghmaei-Sabegh, E. Bojórquez, Three-dimensional response of steel moment-resisting buildings under seismic sequences, Engineering Structures, 175 (2018) 399-414.

[34] G. Wang, Y. Wang, W. Lu, P. Yan, M. Chen, Earthquake Direction Effects on Seismic Performance of Concrete Gravity Dams to Mainshock–Aftershock Sequences, Journal of Earthquake Engineering, (2018) 1-22.

[35] W. Wen, D. Ji, C. Zhai, Ground motion rotation for mainshock-aftershock sequences: Necessary or not?, Soil Dynamics and Earthquake Engineering, 130 (2020) 105976.

[36] F. Hosseinpour, A.E. Abdelnaby, Effect of different aspects of multiple earthquakes on the nonlinear behavior of RC structures, Soil Dynamics and Earthquake Engineering, 92 (2017) 706-725.

[37] L. Di Sarno, S. Amiri, A. Garakaninezhad, Effects of incident angles of earthquake sequences on seismic demands of structures, Structures, 28 (2020) 1244-1251.

[38] S. Amiri, L. Di Sarno, A. Garakaninezhad, On the aftershock polarity to assess residual displacement demands, Soil Dynamics and Earthquake Engineering, 150 (2021) 106932.

[39] K. Kostinakis, A. Athanatopoulou, K. Morfidis, Correlation between ground motion intensity measures and seismic damage of 3D R/C buildings, Engineering Structures, 82 (2015) 151-167.

[40] C. Yang, L. Xie, A. Li, J. Jia, D. Zeng, Ground motion intensity measures for seismically isolated RC tall buildings, Soil Dynamics and Earthquake Engineering, 125 (2019) 105727.

[41] V. Jahangiri, M. Yazdani, M.S. Marefat, Intensity measures for the seismic response assessment of plain concrete arch bridges, Bulletin of Earthquake Engineering, 16 (2018) 4225-4248.

[42] C. Zelaschi, R. Monteiro, R. Pinho, Critical Assessment of Intensity Measures for Seismic Response of Italian RC Bridge Portfolios, Journal of Earthquake Engineering, 23 (2019) 980-1000.

[43] J. Zhong, J.-S. Jeon, Y.-H. Shao, L. Chen, Optimal Intensity Measures in Probabilistic Seismic Demand Models of Cable-Stayed Bridges Subjected to Pulse-Like Ground Motions, Journal of Bridge Engineering, 24 (2019) 04018118.

[44] J. Guo, M.S. Alam, J. Wang, S. Li, W. Yuan, Optimal intensity measures for probabilistic seismic demand models of a cable-stayed bridge based on generalized linear regression models, Soil Dynamics and Earthquake Engineering, 131 (2020) 106024.

[45] H. Shakib, V. Jahangiri, Intensity measures for the assessment of the seismic response of buried steel pipelines, Bulletin of Earthquake Engineering, 14 (2016) 1265-1284.

[46] A. Kiani, M. Torabi, S.M. Mirhosseini, Intensity measures for the seismic response evaluation of buried steel pipelines under near-field pulse-like ground motions, Earthquake Engineering and Engineering Vibration, 18 (2019) 917-931.

[47] G. Tsinidis, L. Di Sarno, A. Sextos, P. Furtner, Optimal intensity measures for the structural assessment of buried steel natural gas pipelines due to seismically-induced axial compression at geotechnical discontinuities, Soil Dynamics and Earthquake Engineering, 131 (2020) 106030.

[48] W. Wen, C. Zhai, D. Ji, S. Li, L. Xie, Framework for the vulnerability assessment of structure under mainshock-aftershock sequences, Soil Dynamics and Earthquake Engineering, 101 (2017) 41-52.

[49] S. Tesfamariam, K. Goda, Energy-Based Seismic Risk Evaluation of Tall Reinforced Concrete Building in Vancouver, BC, Canada, under Mw9 Megathrust Subduction Earthquakes and Aftershocks, Frontiers in Built Environment, 3 (2017).

[50] N. Shome, C.A. Cornell, P. Bazzurro, J.E. Carballo, Earthquakes, records, and nonlinear responses, Earthquake Spectra, 14 (1998) 469-500.

[51] N. Luco, C.A. Cornell, Structure-specific scalar intensity measures for near-source and ordinary earthquake ground motions, Earthquake Spectra, 23 (2007) 357-392.

[52] Pacific Earthquake Engineering Research Center. PEER Ground Motion Database, (https://ngawest2.berkeley.edu/), in.

[53] K. SL, Geotechnical earthquake engineering, Englewood Cliffs: Prentice Hall, 1996.

[54] G.W. Housner, Strong Ground Motion. In Earthquake Engineering, Prentice-Hall Inc., 1970.

[55] A. Arias, A measure of earthquake intensity, inSeismic Design forNuclear Power Plants, R. J. Hansen (Editor), The MIT Press, Cam-bridge, Massachusetts, 1970.

[56] J.J. Bommer, A. MartÍNez-Pereira, The effective duration of earthquake strong motion, Journal of Earthquake Engineering, 3 (1999) 127-172.

[57] J.R. Benjamin, A criterion for determining exceedances of the operating basis earthquake, Epri report np-5930, Electric Power Research Institute, Palo Alto, (1988).

[58] I.M. Taflampas, C.C. Spyrakos, I.A. Koutromanos, A new definition of strong motion duration and related parameters affecting the response of medium–long period structures, Soil Dynamics and Earthquake Engineering, 29 (2009) 752-763.

[59] R. Dobry, I. Idriss, E. Ng, Duration characteristics of horizontal components of strong-motion earthquake records, Bulletin of the Seismological Society of America, 68 (1978) 1487-1520.

[60] Y.J. Park, A.H.S. Ang, Y.K. Wen, Seismic Damage Analysis of Reinforced Concrete Buildings, Journal of Structural Engineering, 111 (1985) 740-757.

[61] C.A. Cornell, F. Jalayer, R.O. Hamburger, D.A. Foutch, Probabilistic basis for 2000 SAC federal emergency management agency steel moment frame guidelines, Journal of structural engineering, 128 (2002) 526-533.